RESEARCH PAPER

Dynamics of spark cavitation bubbles in a microchamber

Zeheng Jiao[1,2,3] · Jingjing Zhao[4] · Yong Han[1,2,3] · Zixi Chao[1,2,3] · Zheng You[1,2,3]

Abstract

In recent years, more and more actuators based on cavitation bubbles are developed for microfluidic chips to implement various functions, such as sorting cells and mixing the flows. However, the dynamic properties of cavitation bubbles in microfluidic chips have not been systematically studied. Using voltage-controlled sparks to trigger cavitation bubbles in a microfluidic chamber, this work studies the relationship between the bubble size and the input energy, the effect of the aqueous solution conductivity on the bubble size, the repeated spark actions, and the necessity of the buffer flow to keep the repeated cavitation steady. The findings in this work reveal how to generate individual cavitation bubble inside microfluidic chips in a controllable way, which can contribute to creating new microfluidic actuators driven by cavitation bubbles.

1 Introduction

Cavitation bubble is first found in turbomachinery in the nineteenth century. The oscillation dynamics of a largely free cavitation bubble in homogeneous medium is governed by the well-known Rayleigh–Plesset equation (Plesset and Zwick 1954), which can consummately predict bubble radius and lifetime, while the study of the cavitation bubble in the microfluidic environment is relatively lacking.

Recently, micro cavitation bubbles have been successfully utilized as various microfluidic actuators in the field of microfluidics. For example, on-chip cell sorters are developed using the transient force of the jet flow of an expanding cavitation bubble (Zhao and You 2018; Meng 2020; De 2017; Wu 2012). Also, cavitation bubbles are applied for micro mixing with the ability of stirring and stretching the flows (Surdo et al. 2017; Orbay 2017; Dong 2017; Ozcelik

2014), and can rupture the lipid membranes for vesicle deformation and lysis (Li 2013; Marmottant and Hilgenfeldt 2003; Gac 2007). Pulsed laser(Chen 2013; Iino 2019; Zhang 2011), microheater (De 2017; Yuan et al. 1999), ultrasonic (Orbay 2017; Hashmi 2012; Shchukin 2011; Tandiono et al. 2010), hydrodynamics (Falcucci 2013; Medrano, et al. 2011; Shang 2016), and electric spark (Zhao and You 2018; Fong 2009; Shan 2019) are major methods for generation of on-chip cavitation bubbles.

Confined by the walls, the cavitation bubble in the microfluidic chip features the very different dynamic properties in comparison with the bubble in the infinite fluid. It is necessary to study the bubble evolution in the confined environment for controllable bubble use. Prosperetti (Yuan et al. 1999) researched on the growth and collapse of a vapor bubble generated by an on-chip microheater in a small tube and summarized how the internal pressure and external pressure govern the bubble dynamics. Ohl and Ohl (2016) investigated the generation, dynamics, and applications of acoustic bubbles in a microchannel. Ed Zwaan (2007) reported the dynamics of a cavitation bubble occurring in a narrow gap which are surrounded by additional boundaries. Quinto-Su et al. (2009) and Gonzalez-Avila (2011) presented experimental results of bubble dynamics inside a narrow gap with variable height. The cavitation bubbles in these three studies are created by pulsed lasers. All the studies mentioned above establish the basis of bubble dynamics in microfluidic systems. However, some details are neglected, such as the influence from deposited energy and solution characteristics, also the study of repeated cavitation.

✉ Jingjing Zhao
zhaojj@stanford.edu

✉ Zheng You
yz-dpi@mail.tsinghua.edu.cn

1 State Key Laboratory of Precision Measurement Technology and Instrument, Tsinghua University, Beijing 100084, China

2 Department of Precision Instrument, Tsinghua University, Beijing 100084, China

3 Beijing Laboratory for Biomedical Detection Technology and Instrument, Tsinghua University, Beijing 100084, China

4 Department of Structural Biology, School of Medicine, Stanford University, Stanford, CA 94305-5126, USA

This paper studies the cavitation bubble dynamics in a microfluidic environment in terms of the time evolution of the bubble, influence of the solution conductivity, the bubble energy, and repeated cavitation. Electric spark is used to trigger bubbles. This generation method does not need neither the expensive setup and precise optical calibration required for pulsed laser, nor the sophisticated fabrication of microheater, and has a better spatial resolution than ultrasonic method dose. By applying a controlled high-voltage discharge on the electrodes in the microfluidic chip, a dielectric breakdown of liquids between the electrodes comes into being, the deposited energy of which brings in localized heat and high-pressure, consequently producing a controllable cavitation bubble (Dhanik and Joshi 2005).

2 Experimental setup

Figure 1a shows the microfluidic chip composed of three layers. The glass plates and metal electrodes (stainless-steel/tungsten) are processed by laser engraving, integrated with UV adhesive bonding (Fig. S1). The inner glass plate is 150 μm thick, with the designed microchamber and channels. The 1 mm glass plates serve as covers for protection, observation and fluid connection. The thickness of electrodes is the same with that of the inner glass plate.

The thin needle-like structure and the arc-shaped parts are positive electrode (PE) and negative electrodes (NE), respectively. In the microchamber surrounded by the electrodes and glass plates, the electric field is simulated by finite element analysis (COMSOL Multiphysics 5.5). As shown in Fig. 1b, electric field ascends dramatically near the tip of PE, where the maxima exist. As a result, dielectric breakdown first initiates there in a spark discharge and the spark cavitation bubble is only generated adhere to the PE. This design accurately determines the location of the cavitation bubble. The channel connected to the chamber is designed for buffer flow to refresh liquids in the repeated cavitation experiment. The high-voltage circuit for the spark discharge is shown in Fig. 1c. A digital function generator is responsible for rectangle pulses. For each pulse given to the N-MOS, a high-voltage electric discharge with the same duration is applied on the electrodes. The operation limit of the device is 1000 times for *stainless-steel* electrodes and 10,000 times for tungsten electrodes (Fig. S2). Bubble dynamics is recorded by a high-speed camera (Photron FastCam SA-Z, Photron Inc., Japan) at 200,000 frames per second (fps). An LED flashlight is for illumination (Fig. 1d).
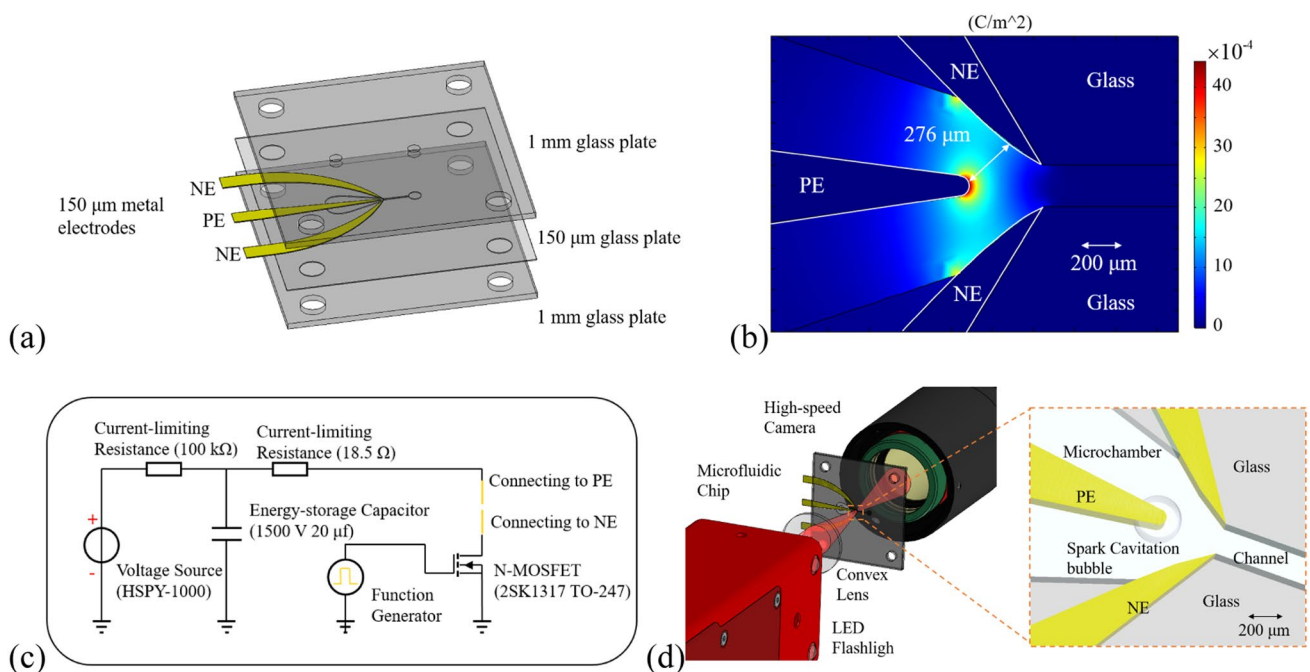

Fig. 1 **a** The three-layer structure of the microfluidic chip. **b** Electric field derived by finite element analysis, 550 V is applied on the PE. The minimum distance between two electrodes is 276 μm. **c** High-voltage circuit for spark discharge. **d** A high-speed camera and a LED flashlight are used to record the bubble dynamics

3 Experimental results

To explore the dynamic behavior of an on-chip spark cavitation bubble, we conduct the experiments in the following steps. We measure the time evolution of bubble radius for the first step, and then analyze the relationship of bubble maximum volume and lifetime, both of which are the major parameters to describe a cavitation bubble. Next, we study the discharge energy versus bubble maximum volume and apply different concentrations of PBS in the experiment to explore the influence of solution conductivity on the bubble dynamics. Last, we apply a series of spark discharges on the electrodes to create repeated cavitation and analyze the bubble dynamics under different discharge frequencies and buffer flowrates.

3.1 Time evolution of the bubble radius

To understand the cavitation bubble dynamics in a microfluidic chamber, it is essential to first analyze the time evolution of bubble volume and radius. The microfluidic chip is filled with phosphate buffer saline ($1 \times$ PBS, ionic strength 162.7 mM) to reduce voltage threshold for bubble generation. The discharge voltage is set as 550 V, and the discharge

duration ranges from 2 to 22 μs to generate different sized bubbles. Figure 2a shows a typical bubble time evolution image (more detailed time evolution images with shorter time interval are shown in Fig. S3). The discharge duration is 14 μs. The bubble first expands three-dimensionally. After reaching upper and lower walls of the microchamber, the bubble turns into a pancake shape and exhibits a two-dimensional planar expansion. (Fig. S4 explains how to determine if the bubble reaches upper and lower walls). Confined by the positive electrode, it then develops to non-radial shape, especially during its collapse phase. High-speed movies of bubbles are analyzed frame-by-frame using ImageJ, as shown in Fig. S5a. Here, we define equivalent radius R as $R = (S/\pi)^{1/2}$, where S is projected area of the bubble, schematically shown in Fig. S5b. Figure 2b shows the equivalent radius versus time of five different sized bubbles. We find that the expansion phase of the bubble is slightly faster than the collapse phase. To compare these various different sized bubbles, the equivalent radius is normalized by R_{max}, and time is normalized by bubble lifetime T. Figure 2c shows that generally all bubble normalized radii are in good correlation, independent to the discharge duration. This indicates that the expansion and collapse of different size bubbles share a similar pattern. Namely, the bubble dynamics can be epitomized by two major parameters that
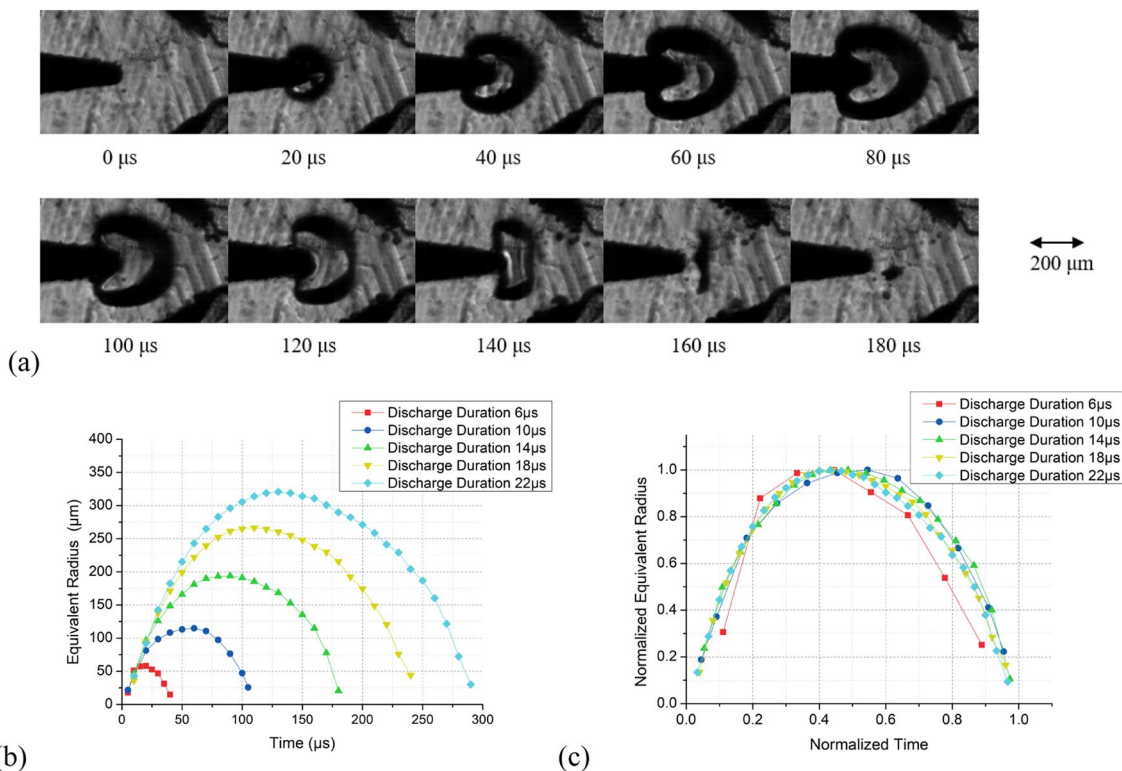

Fig. 2 **a** Time evolution of a bubble with a discharge duration of 14 μs. **b** Equivalent radius verse time of different sized bubble. **c** Normalized equivalent radius verse time for the cases shown in **b**

can distinguish different bubbles, the maximum equivalent radius R_{max} and the lifetime T. In the following analysis, we will focus on these two parameters rather than entire time evolution data. It is noticeable that in Fig. 2c, the curve of the bubble with 6 μs discharge duration is slightly different from the others. The main reason is that its radius is so small that the bubble only goes through three-dimensional expansion and collapse. Another potential reason is that there is some uncertainty in the zero of the curves due to the timing between frames.

3.2 Maximum equivalent radius and lifetime.

The growth and collapse of a spark cavitation bubble in the infinite homogeneous and incompressible fluid has been studied by many researchers. The well-known Rayleigh equation for the three-dimensional spherical cavitation bubble (Chahine et al. 1995; Leighton 2011) is written as

$$R\ddot{R} + \frac{3}{2}\dot{R} = \frac{p}{\rho}, \tag{1}$$

where R is the bubble radius. ρ and p represent the density of the fluid and pressure in liquid far from the bubble, respectively. For simplicity, if we neglect vapor pressure within the bubble and the fluid, by demanding a balance between kinetic energy in the fluid when the liquid collapse into the cavitation bubble and the work done by fluid in compressing the cavity, collapse time of the bubble is obtained as $\tau_{collapse} = 0.915R_{max}\left(\frac{\rho}{p}\right)^{1/2}$. The expansion phase is assumed to be a mirror image of the collapse phase. Thus, lifetime of the cavitation bubble in infinite region is $\tau_{inf} = 2\tau_{collapse} = 1.83R_{max}\left(\frac{\rho}{p}\right)^{1/2}$ (Cook 1993).

As is discussed before, spark cavitation bubbles in a microchamber first expands three-dimensionally, and then two-dimensionally after reaching upper and lower walls of

the chamber. The dynamics equation for the two-dimensional bubble collapse (Zwaan 2007; Lohse 2004) is

$$R\ddot{R} + \dot{R}^2 \log\frac{R}{R_\infty} = \frac{p}{\rho}, \tag{2}$$

where R_∞ is defined by the distance where the fluid velocity drops to zero. Due to the difficulty to accurately determine R_∞, it is hard to get the analytical solution. We have done finite element analysis via COMSOL Multiphysics 5.5 (2D, two-phase flow, moving mesh, more details can be found in Fig. S6) to analyze the two-dimensional expansion and collapse of different sized bubbles. Also, we analyze the high-speed movies of the bubbles in Sect. 3.1 (550 V discharge voltage, discharge duration from 2 to 22 μs) and measure their lifetimes and maximum equivalent radii. Figure 3a compares the experimental results with the simulation results. Confined by the walls and electrodes, with the same lifetime, the on-chip spark cavitation bubble reaches a much smaller maximum radius in comparison to the bubble in infinite homogeneous incompressible fluid. Less affected by upper and lower walls of the chamber, the bubble with a maximum radius less than 50 μm has an evolution process more similar to that of the bubble in infinite fluid. Its expansion and collapse phases are quicker than those predicted by 2D FEA simulation. The bubble with large radius reaches upper and lower walls, and the experimental curve resembles the 2D simulated curve, the curve gradients of which are coincident.

3.3 Discharge duration and projected area

For a spark cavitation bubble, the kinetic energy E_k vanishes when the radius reaches the maximum, $R = R_{max}$. At this moment, the potential energy is $E_p = V_{max}p$, where V_{max} is the maximum volume and p represents the pressure in the liquid far from the bubble. The total energy of
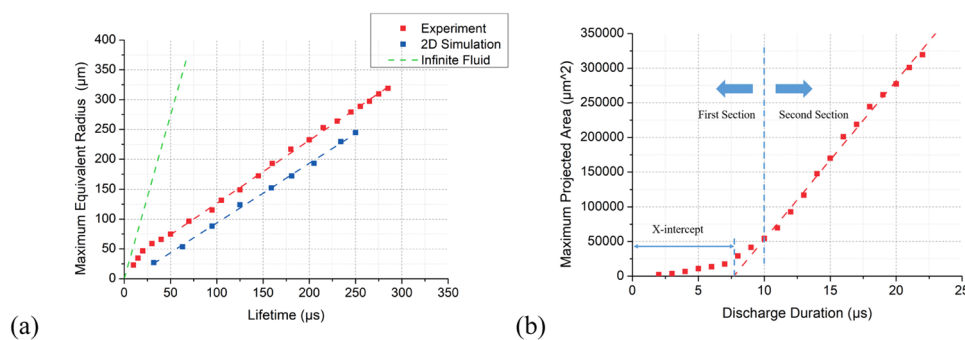

(a)

(b)

Fig. 3 **a** Lifetime and maximum equivalent radius of a cavitation bubble. Markers are from measurements with the high-speed camera or simulations via COMSOL Multiphysics. The green dashed line rep-

resents spherical bubbles in infinite homogeneous incompressible fluid. **b** Maximum projected area of bubbles generated by the spark discharges of different durations

the cavitation bubble is $E = E_p + E_k = V_{max}p$ (Cook 1993). The hydraulic efficiency is defined as $\varepsilon_{hyd} = E/E_{discharge}$, where $E_{discharge}$ is the energy delivered by the electric discharge. Thus, the relationship between $E_{discharge}$ and V_{max} is

$$V_{max} = \frac{\varepsilon_{hyd}}{p}E_{discharge}. \tag{3}$$

Due to the complex bubble dynamics and energy transformation, there are very few literatures discussing the relationship between input energy and volume of an on-chip cavitation bubble. Some literatures discussed the input energy and dynamics of microjets induced by the cavitation bubbles (Tagawa 2012; Berrospe-Rodriguez et al. 2016). Prosperetti (Yuan et al. 1999) studied the correlation between bubble volume and initial liquid superheat of a cavitation bubble in a small tube. Here we try to experimentally explore and give a quantitative conclusion between input energy and bubble volume of a cavitation bubble in a microchamber.

At a fixed discharge voltage, the current through the electrodes is almost constant during a spark discharge (Fig. S7). The energy of the electrical discharge depends on discharge duration, giving $E_{discharge} = UIt_{discharge}$, where $t_{discharge}$ is the discharge duration. We measured the maximum projected area S_{max} of the bubbles in Sect. 3.1 (discharge voltage 550 V, discharge duration varied from 2 to 22 μs) (Fig. 3b). The curve is divided into two sections according to different gradients. First section consists of the bubbles with discharge durations less than 10 μs, while in second section, the bubbles are triggered with discharge durations longer than 10 μs.

First, spark cavitation bubbles in the second section are discussed. Those bubbles are large enough to reach upper and lower walls of the chamber and expand two-dimensionally. The maximum volume V_{max} is $V_{max} = S_{max}h$ and h is the chamber height. Equation (3) takes the form of the following equation:

$$S_{max} = \frac{\varepsilon_{hyd}UI}{ph}t_{discharge}. \tag{4}$$

The linear relationship between $t_{discharge}$ and S_{max} is demonstrated by experimental results, with $R^2 = 0.995$. There is an x-intercept in the linear fitting of S_{max} and $t_{discharge}$. We surmise that it is a threshold value representing the energy consumed for dielectric breakdown and forming of the conductive path. This part of the energy, $E_{breakdown}$, is not directly contributive to the cavitation bubble. If we exclude $E_{breakdown}$ from $E_{discharge}$, S_{max} is proportional to $\left(UIt_{discharge} - E_{breakdown}\right)$ as $S_{max} = \frac{\varepsilon_{hyd}}{ph}\left(UIt_{discharge} - E_{breakdown}\right)$. An almost constant hydraulic efficiency of $\varepsilon_{hyd} \approx 1.15 \times 10^{-3}$ is derived from the slope of the linear fitting.

As for spark cavitation bubbles in the first section in Fig. 3b, according to the theory developed by Cook (Cook 1993; Roberts 1996), a small portion of the discharge energy is delivered to the cavitation bubble before main discharge starts. This pre-discharge energy is responsible for initiating tiny cavitation bubbles. This theory may explain why the spark energy lower than the threshold value can also create a small cavitation bubble in the first section.

Additionally, experiments with fixed discharge duration and varied discharge voltages are carried out. Similar curve between maximum projected area of bubbles and discharge energy is found, as shown in Fig. S8.

3.4 Electrical conductivity of aqueous solution and maximum projected area

The electrical conductivity of aqueous solution is another important factor that influences the bubble dynamics. We have done experiments with different concentrations of PBS (ionic strength is listed in Table 1) to explore the bubble dynamics with variable solution conductivities.

The discharge voltage is fixed at 550 V, and the discharge duration varies from 0.5 to 34 μs. The curves describing the relationships between $t_{discharge}$ and S_{max} are diagramed in Fig. 4a. The curve gradients are relatively low with short discharge durations, then increase and remain stable after the discharge duration surpasses a certain threshold. Higher concentration of PBS with a higher ionic strength results in an easier electrical breakdown, a lower after-breakdown resistance value between electrodes and a shorter discharge duration required for a specific bubble size. The currents through the electrodes are measured to estimate discharge energy. Figure 4b shows that the curves of different PBS concentrations are close, except for the spark discharge with 0.5×PBS. The 0.5×PBS features an extremely low conductivity, making the discharge duration much longer. The low hydraulic efficiency of this test is $\varepsilon_{hyd} \approx 6 \times 10^{-4}$, much smaller than those of other concentrations. We have also done experiments with different concentration of sodium chloride. The result is shown in Fig. S9.

3.5 Repeated cavitation

Some microfluidic requires spark cavitation bubbles to be produced repeatedly, such as micro mixing (Surdo et al. 2017) and cell sorting (Zhao and You 2018). Repeated cavitation is much more complicated than single cavitation because of

Table 1 Ionic strengths with different concentrations of PBS

Concentrations of PBS	0.5×	1×	2×	5×	10×
Ionic strength (mM)	81.35	162.7	325.4	813.5	1627.0

Fig. 4 a Maximum projected area of the spark bubbles versus discharge duration for different aqueous solution conductivities. The discharge voltage is fixed at 550 V and five different concentrations of PBS are tested. **b** Maximum projected area of the spark bubbles in **a** versus discharge energy
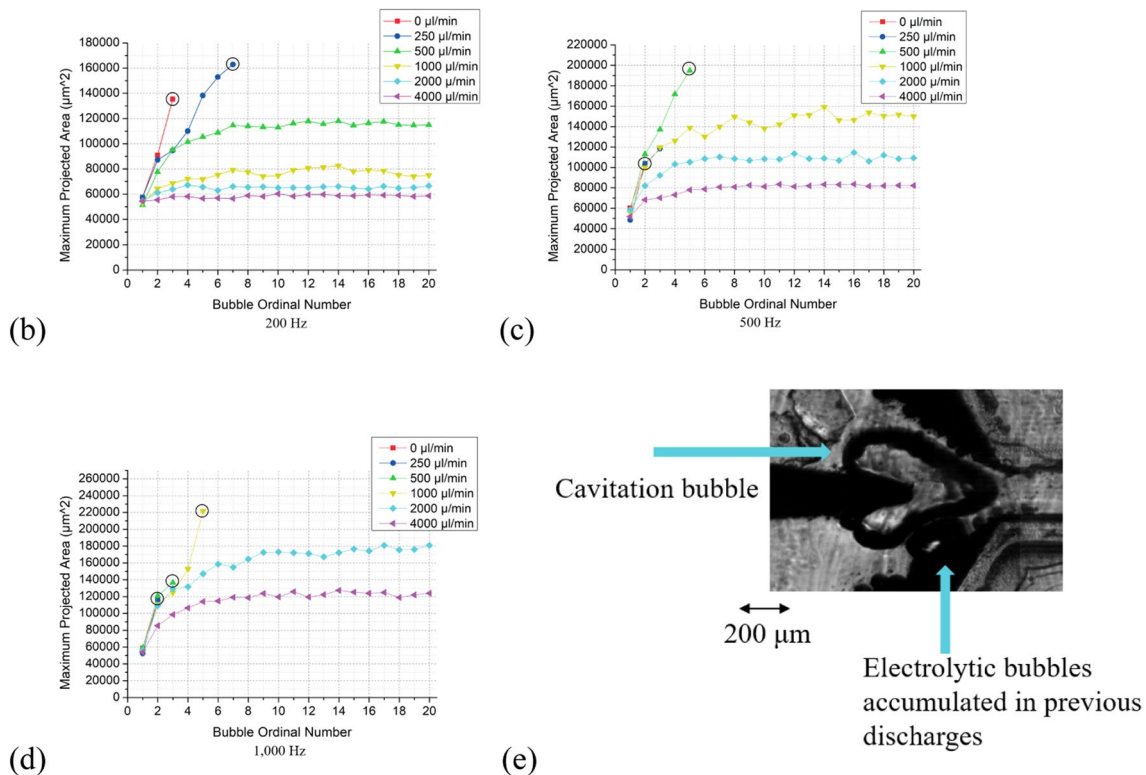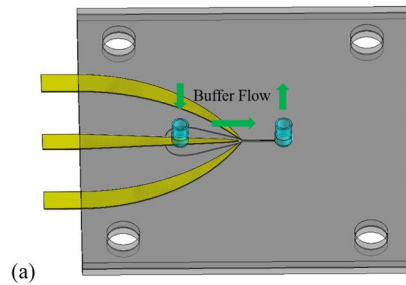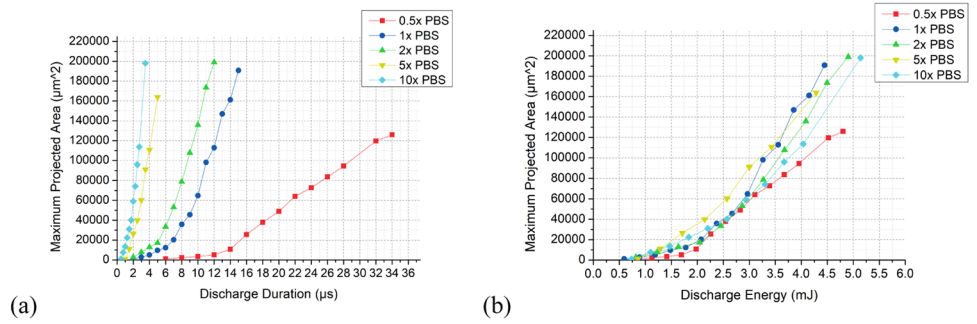

(a)

(b)

(a)

(b)

(c)

(d)

(e)

Fig. 5 a Flow direction of the buffer flow. **b–d** Maximum projected area of 20 repeated cavitation bubbles under different spark frequencies. **e** When the pulse frequency is high and the buffer flowrate is low, electrolytic bubbles accumulate easily between electrodes. Those bubbles interfere, squeeze, and deform the later cavitation bubble. The black circles in **b–d** mean that the following cavitation bubbles in the tests are seriously influenced by the accumulated bubbles and the following data are not shown

Table 2 Two criteria to evaluate the washing efficiency of the buffer flow, three different pulse frequencies and six different flowrates of buffer flow are tested

Frequency of spark discharge	200 Hz	500 Hz	1000 Hz
Buffer flowrate (µl/min)			
0	No	No	No
250	No	No	No
500	Yes, $\beta = 2.26$	No	No
1000	Yes, $\beta = 1.48$	Yes, $\beta = 2.67$	No
2000	Yes, $\beta = 1.20$	Yes, $\beta = 1.88$	Yes, $\beta = 3.13$
4000	Yes, $\beta = 1.08$	Yes, $\beta = 1.59$	Yes, $\beta = 2.30$

Yes the buffer flow is sufficient to sweep away the electrolytic bubbles and to prevent them from accumulating, *No* the buffer flow is not sufficient

two consequent defects. The first is that, many tiny electrolytic bubbles (Chahine et al. 1995; Bhattacharyya et al. 1999) (H_2 and O_2) are created concomitantly at both positive and negative electrodes during a spark discharge. Those electrolytic bubbles will accumulate around the electrodes to enhance the subsequent cavitation. The second is that the electrical breakdown increases the conductivity of aqueous solution between electrodes, making the later cavitation bubbles larger and larger because of a higher solution conductivity (referring to Sect. 3.4). To keep a steady and controllable repeated cavitation, a buffer flow is applied to wash the cavitation region using a syringe pump (Fig. 5a), aiming to wash away undesired bubbles and restore solution conductivity. The discharge voltage and duration are set to be 550 V and 10 µs. 1×PBS solution is used. Three different pulse frequencies and six different flowrates of buffer flow are tested, as shown in Fig. 5b–d. For each test, the digital function generator is applied to generate a series of 20 pulses at one time.

Two criteria are introduced to evaluate the washing efficiency of the buffer flow. First is to see whether the buffer flow is sufficient enough or not to sweep away the electrolytic bubbles to prevent them from accumulating and affecting the later cavitation bubbles. If yes, then the second criterion is the coefficient of enlargement β, which is defined as $\beta = \frac{S_{max}}{S_{max\,1st}}$ by comparing the average S_{max} of the 11th–20th bubbles with that of the 1st bubble. A small β indicates that the solution conductivity near electrodes is stable and the washing efficiency is high. As listed in Table 2, the increase of S_{max} during repeated operation is universal. Even at low spark frequency (200 Hz) and high buffer flowrate (4000 µl/min), we still observe a slight increase in S_{max} between the later bubbles and the first bubble ($\beta = 1.08$). A higher spark discharge frequency demands a higher buffer flowrate. In other words, a higher flowrate can achieve a better washing efficiency under the same discharge frequency. It can be concluded that for microfluidic

applications where the controllable and stable cavitation is created periodically, it is important to refresh the region between electrodes with an adequate buffer flow. The flowrate of the buffer can be decided according to the coefficient of enlargement. Generally, the minimum requirement is to sweep away most of the electrolytic bubbles to prevent them from accumulating.

4 Conclusion

In this work, the dynamics of spark cavitation bubbles in a microchamber is investigated in detail. The input/output parameters of a spark cavitation bubble are systematically studied. These experimental results shed lights on the future design of microfluidic actuators using cavitation bubbles, especially for the repeated spark cavitation microbubbles. It reveals the importance of the buffer flow on holding the repeated cavitation steady. Two criteria are proposed to help researchers select the appropriate flowrate of buffer flow. Theoretically, one effective method to reduce electrolysis during spark discharge is to increase the discharge voltage to several kV (Nguyen et al. 2012), resulting in a much shorter discharge duration for the same amount of energy needed for a cavitation bubble, which is beneficial to the stability of repeated cavitation. Currently, the cavitation bubble is designed as a rapid and convenient actuator (Hashmi 2012; Quinto-Su 2010; Dijkink and Ohl 2008; Ogunyinka 2020; Gao 2020) in different microfluidic applications such as cell sorting (Zhao and You 2018; Meng 2020; De 2017; Wu 2012), micro mixing (Surdo et al. 2017; Orbay 2017; Dong 2017; Ozcelik 2014), and cell lysis (Li 2013; Marmottant and Hilgenfeldt 2003). Our work on the cavitation bubble dynamics in the microfluidic environment can show new insights into the applications of on-chip cavitation bubbles.

References

Berrospe-Rodriguez C et al (2016) Continuous-wave laser generated jets for needle free applications. Biomicrofluidics 10(1):1932–1058. https://doi.org/10.1063/1.4940038

Bhattacharyya B, Doloi BN, Sorkhel SK (1999) Experimental investigations into electrochemical discharge machining (ECDM) of non-conductive ceramic materials. J Mater Process Technol 95(1–3):145–154

Chahine G et al (1995) Spark-generated bubbles as laboratory-scale models of underwater explosions and their use for validation of

simulation tools. In: SAVIAC proceedings of the 66th shock and vibrations symposium

Chen Y et al (2013) 3D pulsed laser-triggered high-speed microfluidic fluorescence-activated cell sorter. Analyst 138(24):7308–7315

Cook JA (1993) Interaction of multiple spark-generated bubbles in a compressible liquid. Texas Univ at Austin Applied Research Labs, Austin

De WK et al (2017) Micro vapor bubble jet flow for safe and high-rate fluorescence-activated cell sorting. Lab Chip 17(7):1287–1296

Dhanik S, Joshi SS (2005) Modeling of a single resistance capacitance pulse discharge in micro-electro discharge machining. J Manufact Sci Eng Trans ASME 127(4):759–767

Dijkink R, Ohl CD (2008) Laser-induced cavitation based micropump. Lab Chip 8(10):1676–1681

Dong ZY et al (2017) Mixing and Residence Time Distribution in Ultrasonic Microreactors. AIChE J 63(4):1404–1418

Falcucci G et al (2013) Direct numerical evidence of stress-induced cavitation. J Fluid Mech 728:362–375

Fong SW et al (2009) Interactions of multiple spark-generated bubbles with phase differences. Exp Fluids 46(4):705–724

Gao Y et al (2020) Acoustic bubble-based bidirectional micropump. Microfluid Nanofluid 24(4):10

Gonzalez-Avila SR et al (2011) Cavitation bubble dynamics in a liquid gap of variable height. J Fluid Mech 682:241–260

Hashmi A et al (2012) Oscillating bubbles: a versatile tool for lab on a chip applications. Lab Chip 12(21):4216–4227

Iino T et al (2019) High-speed microparticle isolation unlimited by Poisson statistics. Lab Chip 19(16):2669–2677

Le Gac S et al (2007) Sonoporation of suspension cells with a single cavitation bubble in a microfluidic confinement. Lab Chip 7(12):1666–1672

Leighton TG (2011) The inertial terms in equations of motion for bubbles in tubular vessels or between plates. J Acoust Soc Am 130(5):3333–3338

Li ZG et al (2013) Single cell membrane poration by bubble-induced microjets in a microfluidic chip dagger. Lab Chip 13(6):1144–1150

Lohse D et al (2004) Impact on soft sand: void collapse and jet formation. Phys Rev Lett 93(19):4

Marmottant P, Hilgenfeldt S (2003) Controlled vesicle deformation and lysis by single oscillating bubbles. Nature 423(6936):153–156

Medrano M et al (2011) Hydrodynamic cavitation in microsystems. I. Experiments with deionized water and nanofluids. Phys Fluids 23(12):13

Meng L et al (2020) Microbubble enhanced acoustic tweezers for size-independent cell sorting. Appl Phys Lett 116(7):5

Nguyen MD, Rahman M, Wong YS (2012) An experimental study on micro-EDM in low-resistivity deionized water using short voltage pulses. Int J Adv Manuf Technol 58(5–8):533–544

Ogunyinka O et al (2020) An integrated microfluidic chip for generation and transfer of reactive species using gas plasma. Microfluid Nanofluid 24(2):16

Ohl SW, Ohl CD (2016) Acoustic cavitation in a microchannel. Springer, Singapore, pp 99–135

Orbay S et al (2017) Mixing high-viscosity fluids via acoustically driven bubbles. J Micromech Microeng 27(1):6

Ozcelik A et al (2014) An acoustofluidic micromixer via bubble inception and cavitation from microchannel sidewalls. Anal Chem 86(10):5083–5088

Plesset MS, Zwick SA (1954) The growth of vapor bubbles in super-heated liquids. J Appl Phys 25(4):493–500

Quinto-Su PA, Lim KY, Ohl CD (2009) Cavitation bubble dynamics in microfluidic gaps of variable height. Phys Rev E 80(4):4

Quinto-Su PA et al (2010) Manipulation and microrheology of carbon nanotubes with laser-induced cavitation bubbles. PHYS Rev Lett 104(1):4

Roberts RM et al (1996) The energy partition of underwater sparks. J Acoust Soc Am 99(6):3465–3475

Shan ML et al (2019) Electric characteristic and cavitation bubble dynamics using underwater pulsed discharge. Plasma Sci Technol 21(7):7

Shang LR et al (2016) Osmotic pressure-triggered cavitation in microcapsules. Lab Chip 16(2):251–255

Shchukin DG et al (2011) Ultrasonic Cavitation at Solid Surfaces. Adv Mater 23(17):1922–1934

Surdo S, Diaspro A, Duocastella M (2017) Micromixing with spark-generated cavitation bubbles. Microfluid Nanofluidics 21(5):82

Tagawa Y et al (2012) Highly Focused Supersonic Microjets. Physical Review X 2(3):10

Tandiono T et al (2010) Creation of cavitation activity in a microfluidic device through acoustically driven capillary waves. Lab Chip 10(14):1848–1855

Wu TH et al (2012) Pulsed laser triggered high speed microfluidic fluorescence activated cell sorter. Lab Chip 12(7):1378–1383

Yuan H, Oguz HN, Prosperetti A (1999) Growth and collapse of a vapor bubble in a small tube. Int J Heat Mass Transf 42(19):3643–3657

Zhang K et al (2011) Laser-induced thermal bubbles for microfluidic applications. Lab Chip 11(7):1389–1395

Zhao J, You Z (2018) Spark-generated microbubble cell sorter for microfluidic flow cytometry. Cytometry Part A 93(2):222–231

Zwaan E et al (2007) Controlled cavitation in microfluidic systems. Phys Rev Lett 98(25):4